HHS Public Access

Author manuscript

Cell Rep. Author manuscript; available in PMC 2022 May 31.

Published in final edited form as:

Cell Rep. 2021 September 21; 36(12): 109719. doi:10.1016/j.celrep.2021.109719.

Introduction of synaptotagmin 7 promotes facilitation at the climbing fiber to Purkinje cell synapse

Christopher Weyrer[1,2], **Josef Turecek**[1], **Bailey Harrison**[1], **Wade G. Regehr**[1,3,*]

[1]Department of Neurobiology, Harvard Medical School, Boston, MA 02115, USA

[2]Department of Physiology, Development, and Neuroscience, University of Cambridge, Cambridge CB2 3EG, UK

[3]Lead contact

SUMMARY

Synaptotagmin 7 (Syt7) is a high-affinity calcium sensor that is implicated in multiple aspects of synaptic transmission. Here, we study the influence of Syt7 on the climbing fiber (CF) to Purkinje cell (PC) synapse. We find that small facilitation and prominent calcium-dependent recovery from depression at this synapse do not rely on Syt7 and that Syt7 is not normally present in CFs. We expressed Syt7 in CFs to assess the consequences of introducing Syt7 to a synapse that normally lacks Syt7. Syt7 expression does not promote asynchronous release or accelerate recovery from depression. Syt7 decreases the excitatory postsynaptic current (EPSC) magnitude, consistent with a decrease in the initial probability of release (P_R). Syt7 also increases synaptic facilitation to such a large extent that it could not arise solely as an indirect consequence of decreased P_R. Thus, the primary consequence of Syt7 expression in CFs, which normally lack Syt7, is to promote synaptic facilitation.

In brief

The high-affinity calcium sensor synaptotagmin 7 (Syt7) is implicated in many aspects of synaptic transmission. Weyrer et al. find that introducing Syt7 into climbing fibers (CFs), which do normally express Syt7, promotes synaptic facilitation without affecting two other processes associated with Syt7: recovery from depression and asynchronous release.

Graphical Abstract

*Correspondence: wade_regehr@hms.harvard.edu.

AUTHOR CONTRIBUTIONS

C.W., J.T., and W.G.R. conceived the experiments. C.W. conducted or contributed to all experiments, except Figure 1C. J.T. conducted experiments in Figures 1C and 3C. B.H. helped with immunohistochemistry. Intracranial injections were done by C.W., J.T., and B.H. C.W. and J.T. conducted analyses. C.W. made illustrations. C.W., J.T., and W.G.R. wrote the manuscript.

SUPPLEMENTAL INFORMATION

Supplemental information can be found online at https://doi.org/10.1016/j.celrep.2021.109719.

DECLARATION OF INTERESTS

The authors declare no competing interests.

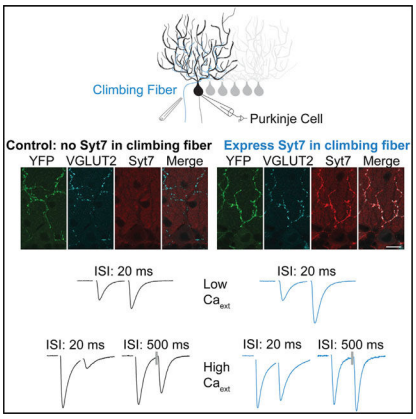

INTRODUCTION

Synaptotagmin 7 (Syt7) contributes in many ways to neurotransmitter release (Huson and Regehr, 2020; MacDougall et al., 2018). First, Syt7 can evoke asynchronous release (AR) of neurotransmitters (Bacaj et al., 2013; Wen et al., 2010). AR persists for several tens of milliseconds following an action potential, it can become prominent during sustained high-frequency activation, and it differs from the typical synchronous release that occurs several milliseconds after an action potential that is mediated by fast Syt isoforms, Syt1 and Syt2 (Fernández-Chacón et al., 2001). Second, Syt7 can interact with calmodulin to promote rapid recovery from depression (Liu et al., 2014). Third, Syt7 can promote facilitation of transmitter release, which is most apparent at synapses where the initial probability of release (P_R) is low (Jackman and Regehr, 2017; Jackman et al., 2016). Fourth, Syt7-dependent facilitation can help to overcome use-dependent depression to make a depressing synapse frequency invariant (Turecek et al., 2017). Fifth, Syt7 can suppress spontaneous vesicle fusion (Luo and Südhof, 2017; Turecek and Regehr, 2019). Finally, Syt7 can decrease the initial P_R (Guan et al., 2020). The effects of expressing Syt7 at a synapse that does not normally contain Syt7 are not known.

Here, we study the role of Syt7 in transmission at the inferior olive climbing fiber (CF) to cerebellar Purkinje cell (PC) (CF→PC) synapse. In adults, each PC typically receives a single CF input. The CF synapse is glutamatergic and consists of hundreds of active zones that provide a powerful excitatory drive (Xu-Friedman et al., 2001). One of the roles of the CF synapse is to gate plasticity of granule cell to PC synapses (Hull, 2020). The CF synapse has also become an important model synapse. It exhibits prominent multivesicular release and postsynaptic glutamate receptor saturation and short-term plasticity (Dittman and Regehr, 1998; Foster et al., 2002; Wadiche and Jahr, 2001). In physiological and elevated external calcium (Ca_e), P_R is very high and CF synapses depress and rapidly recover from depression in a calcium-dependent manner (Dittman and Regehr, 1998; Foster et al., 2002). In low Ca_e, CF→PC synapses facilitate (Foster et al., 2002). It is therefore possible to gain insight into the role of Syt7 in both calcium-dependent recovery from depression and facilitation by studying the CF→PC synapses. We found that CF→PC synapses were unaltered in Syt7 KO mice, indicating that, in wild-type (WT) animals, Syt7

does not play a role in facilitation or recovery from depression at this synapse. This is consistent with our inability to detect Syt7 at the CF synapse.

The lack of Syt7 in CFs suggested that viral Syt7 expression would allow us to assess the effects of Syt7 on transmission at a synapse where it is normally absent. We found that, in low Ca_e, the expression of Syt7 in CFs led to much larger paired-pulse facilitation, decreased excitatory postsynaptic current (EPSC) size, and greatly enhanced facilitation during stimulus trains. In high Ca_e, recovery from depression and AR were unaffected, the extent of paired-pulse depression was greatly reduced, and prolonged paired-pulse facilitation could be observed. These results indicate that introducing Syt7 into this synapse primarily promotes facilitation.

RESULTS

Short-term plasticity at CF synapses is not Syt7 dependent

To determine the role of Syt7 in transmission at the CF→PC synapse, we compared synaptic properties in WT and Syt7 knockout (KO) mice. In physiological Ca_e (1.5 mM), P_R at the CF synapse is high and depression dominates short-term plasticity. Lowering Ca_e greatly reduces initial P_R, thereby reducing depletion and the resulting depression to reveal facilitation (Dittman and Regehr, 1998; Foster et al., 2002). In WT animals in low Ca_e (0.3 mM), paired-pulse facilitation is apparent but small (Figure 1A). Paired-pulse facilitation was unchanged in Syt7 KO mice. In response to a 50-Hz stimulus train, the EPSC continued to grow such that, by the tenth stimulus, there was an almost 3-fold enhancement of synaptic strength in both WT and Syt7 KO mice (Figure 1B). 100-Hz trains produce similar enhancement, and 25-Hz trains produce an approximately 2-fold enhancement (Figure S1). Enhancement in response to stimulus trains was unchanged in Syt7 KO mice (Figure S1). These studies show that facilitation of the CF→PC synapse that is apparent in low Ca_e in WT mice is not mediated by Syt7.

In elevated Ca_e (4 mM), P_R is very high, the CF→PC synapse strongly depresses, and recovery has a rapid and a slow component (Figure 1C). We have previously shown that that the rapid component is calcium dependent, but the slow component is not (Dittman and Regehr, 1998; Foster et al., 2002). Depression and recovery from depression were unchanged in Syt7 KO mice. This indicates that, in WT animals, Syt7 does not play a role in depression or calcium-dependent recovery from depression at CF→PC synapses.

Syt7 is not present at CF synapses in WT animals

It is not clear whether Syt7 is present in CFs but does not play a role in synaptic transmission or whether Syt7 is absent from CFs in WT animals. We initially addressed this issue by using fluorescent *in situ* hybridization to determine whether Syt7 RNA is present in inferior olivary neurons that give rise to CFs (Figure 2A). Probes were used to identify glutamatergic neurons (vGlut1 and vGlut2; magenta) and Syt7 (red). Within the inferior olive (IO), vGlut1/2 labeling was prominent, although Syt7 labeling was not (Figure 2A, left). Images of the hippocampus where Syt7 is known to be prominent in the dentate granule cells and the CA3 region, and to a lesser extent in the CA1 region, serve as a control

(Figure 2A, right). Syt7 and vGlut RNA are both readily detected in the hippocampus. These findings indicate that Syt7 RNA is not present in the excitatory neurons of the IO.

We also used immunohistochemistry to determine whether Syt7 is present in CFs. In WT mice in the molecular layer of the cerebellar cortex, Syt7 was present in the granule cell boutons within the molecular layer (Figure 2B). vGlut2 labeling was used to identify CF synapses, because it is specific to CF synapses within the molecular layer. Merged images show that vGlut2 and Syt7 labeling did not overlap. Thus, we were unable to detect Syt7 in CFs.

Our *in situ* hybridization and immunohistochemistry studies indicate that, in WT animals, Syt7 is not present in IO neurons and cannot be detected presynaptically at CF synapses. This accounts for the observation that transmission at the CF→PC synapse is unaltered in Syt7 KO mice.

Viral expression of Syt7 in IO neurons

The lack of Syt7 in CFs in WT mice makes the CF→PC synapse well suited to assess the effects of Syt7 at a synapse that does not normally express Syt7. We therefore used adeno-associated virus (AAV) to drive bicistronic expression of Syt7 and channelr-hodopsin2-yellow fluorescent protein (ChR2-YFP) in IO neurons (Figures 2C–2F). Injections in the IO (Figure 2C) were used to label IO neurons and their associated CFs with ChR2-YFP (Figure 2F). In control experiments, AAV was used to express ChR2 alone, and Syt7 was absent from these CFs (Figure 2F, top). The YFP tag on ChR2 was used to identify regions receiving infected CFs, and CFs were also optically activated to provide a functional indication of high ChR2 expression levels in the CF (Figures 2D and 2E; see STAR Methods). Paired-pulse optical activation in low Ca_e could evoke CF EPSCs with characteristic facilitation in 0.3 mM Ca_e (Figure 2E, middle). Electrical stimulation led to similar facilitation (Figure 2E, left), and electrical stimulation could facilitate a subsequent optically evoked EPSC (Figure 2E, right). We used optical stimulation to identify adequately infected CF inputs (see STAR Methods) and used electrical stimulation to characterize synaptic responses.

In 0.3 mM Ca_e, Syt7 expression increased the magnitude of facilitation. Paired-pulse facilitation (100 × [paired-pulse ratio (PPR) − 1]) of ChR2-YFP-expressing CFs was approximately 58% (Figure 3A, black; Table S1), which is similar to that observed at WT synapses in the absence of viral expression (~54%; Figure 1A; Table S1). When Syt7 was expressed, there was an approximately 2.5-fold increase in paired-pulse facilitation to approximately 143% (Figure 3A, light blue; Table S1). Syt7 expression had an even more dramatic effect for high-frequency trains (Figures 3B and S2; Table S1). At the end of a 10-stimuli, 50-Hz train, there was a 3.6-fold increase of control synapses and an 11.3-fold increase for Syt7-expressing synapses (Figure 3B; Table S1).

In 4 mM Ca_e, Syt7 expression led to large changes in short-term plasticity. Syt7 expression greatly reduced the extent of paired-pulse depression that is apparent in control synapses (Figure 4A). Remarkably, for inter-stimulus intervals (ISIs) of 100 ms to 4 s, Syt7 expression led to paired-pulse facilitation rather than the depression observed in control

cells for all ISIs. For stimulus trains, the effects of Syt7 expression were only evident early in trains for 50-Hz (Figure 4B) and 10-Hz (Figure 4C) stimulation, although Syt7 expression slightly elevated responses late in 2-Hz trains (Figure 4D).

Facilitation can be altered by directly influencing the mechanism that enhances synapses or indirectly by lowering the initial P_R, thereby decreasing vesicle depletion to increase the extent of facilitation. At some synapses, Syt7 increases facilitation without altering initial P_R, whereas at other synapses, Syt7 increases facilitation by decreasing initial P_R. It is challenging to discriminate between these mechanisms at CF synapses where it is difficult to measure P_R. In order to detect changes in initial P_R, we compared the initial EPSC amplitudes for viral expression of Syt7 and ChR2-YFP to viral expression of ChR2-YFP alone. In 0.3 mM Ca_e, Syt7 expression significantly reduced the initial EPSC by approximately 40% (Figure S3A; Table S1). These findings suggest that viral expression of Syt7 in CFs decreases initial P_R, which could contribute to the Syt7-induced increase in facilitation (see Discussion). In 4 mM Ca_e, Syt7 expression did not statistically alter the initial EPSC amplitudes, although the average amplitude was reduced by 22% (Figure S3B; Table S1).

We also examined the influence of Syt7 on AR and found that the viral expression of Syt7 did not increase AR. The expression of Syt7 also did not result in a slow component of the EPSC indicative of an increase in AR in either 0.3 mM Ca_e (Figure S4) or 4 mM Ca_e (Figure S5). These findings suggest that the expression of Syt7 in CFs does not increase AR.

We also assessed the role of Syt7 in recovery from depression. It is difficult to determine whether Syt7 alters responses evoked by pairs of pulses or trains (Figures 4A–4D) solely by altering facilitation or by also accelerating recovery from depression. We therefore performed experiments to assess the effects of Syt7 on recovery following brief high-frequency trains that deplete the readily releasable pool of vesicles (Figures 4E–4G). In 4 mM Ca_e, the amplitudes of synaptic responses evoked by each stimulus become progressively smaller as a result of high P_R and depletion, and the tenth stimulus evokes an extremely small response. After waiting 500 ms, stimulation with a pair of pulses reveals that the EPSC is recovered to approximately 70% (Table S1) of the initial amplitude, and the second stimulus evokes a strongly depressed response (Figures 4E–4G, black). The expression of Syt7 results in larger responses early in the train, but the responses eventually become extremely small, suggesting the synapse is depleted similarly to control. The lack of a difference in the extent of recovery suggested that expressing Syt7 in this synapse does not change recovery from depression on this timescale (Figures 4E–4G, light blue).

DISCUSSION

Our initial finding was that the prominent calcium-dependent recovery from depression and the small facilitation at the CF→PC synapse are not mediated by Syt7, which is not present in WT mice. The lack of Syt7 in IO neurons allowed us to investigate the effects of introducing Syt7 to a synapse that normally lacks Syt7. Of the many Syt7-dependent influences on synaptic transmission that have been described, we found that the main effect of introducing Syt7 to the CF→PC synapse was to increase facilitation.

Syt7 does not accelerate recovery from depression at CF→PC synapses

Calcium-dependent recovery from depression has been observed at the CF→PC synapse, the calyx of Held synapse, cultured hippocampal cell synapses, and other synapses (Dittman and Regehr, 1998; Stevens and Wesseling, 1998; Wang and Kaczmarek, 1998). This allows synapses to accelerate recovery from depression to meet increased demand when presynaptic firing frequency is elevated. At hippocampal synapses, calcium binds to calmodulin and activates Syt7 to promote recovery from depression (Liu et al., 2014). Syt7 is also thought to accelerate recovery from depression at synapses made by cerebellar molecular layer interneurons (Chen et al., 2017). At the calyx of Held, calcium also activates calmodulin to accelerate recovery from depression (Sakaba and Neher, 2001), but Syt7 did not appear to be involved (Luo and Südhof, 2017). It was therefore unclear whether Syt7 would be involved in recovery from depression at the CF→PC synapse. Our finding that calcium-dependent recovery from depression is prominent at the CF→PC synapse in WT animals and Syt7 KO animals, and that Syt7 is not present in WT animals, establishes that there is a Syt7-independent mechanism that mediates calcium-dependent recovery from depression.

All of the effects of Syt7 expression on PPR and responses evoked by trains are consistent with Syt7 promoting facilitation (Figures 4A–4E). If Syt7 accelerated recovery from depression, then responses evoked late in a stimulus train would be larger (Neher, 2015; Thanawala and Regehr, 2016), but this was not the case for high-frequency stimulations (50 Hz and 10 Hz), where the responses evoked by the sixth to tenth stimulus were unaffected by the expression of Syt7 (Figures 4B and 4C). In addition, Syt7 expression did not significantly affect recovery from depression after a 50-Hz train that appeared to completely deplete the RRP (Figures 4E–4G). Together, these results strongly suggest that Syt7 expression does not influence recovery from depression at the CF→PC synapse.

Syt7 does not mediate AR at CF→PC synapses

Asynchronous release can occur following individual stimuli or during and following a stimulus train. Syt7 has been shown to contribute to both types of asynchronous release at several different types of synapses. For single stimuli or brief bursts of stimuli, AR is particularly prominent when fast Syt isoforms are absent, as in KOs of fast Syt isoforms (Bacaj et al., 2013; Chen et al., 2017; DiAntonio and Schwarz, 1994; Geppert et al., 1994; Kochubey and Schneggenburger, 2011; Littleton et al., 1993; Luo and Südhof, 2017; Sun et al., 2007) at specialized synapses in WT animals (Turecek and Regehr, 2019). Under such conditions, AR is prominent, and the further elimination of Syt7 can eliminate AR, suggesting that Syt7 mediates AR (Bacaj et al., 2013). In many cases, it is possible to quantify AR by observing individual quanta (Atluri and Regehr, 1998; Best and Regehr, 2009), but at some synapses, such as here for the CF→PC synapse, that is impractical because the synapse has a very high probability of release and consists of so many active zones that stimulation evokes the release of so many vesicles that it is impractical to detect individual quanta. For that reason, we have measured the time course of the synaptic current as a means of detecting a slow component that is consistent with AR. Here, even when we express Syt7 presynaptically, we do not observe prominent AR at CF→PC synapses in low external calcium following single stimuli (Figure S4). This adds to the growing list

of synapses where Syt7 is present (in this case virally expressed), but AR following single stimuli is not observed. This may be because the presence of fast Syt isoforms suppresses AR, even when Syt7 is present (Huson and Regehr, 2020).

At some synapses, AR is prominent during and following stimulus trains, and often this AR is mediated, at least partially, by Syt7. It is difficult to determine whether AR occurs during the train, because glutamate pooling and prolonged glutamate signals can prolong synaptic responses independently of AR. The slow synaptic response observed following high-frequency stimulation in high Ca_e (Figures S5E and S5F) might reflect either a persistent glutamate signal or AR. It is expected, however, that if Syt7 expression promotes AR then this component would be large, and this is not the case. Similarly, if Syt7 promoted AR during a 10-Hz stimulus train, then the EPSC time course would be significantly prolonged, and this is not the case (Figure S5G; Table S1). We therefore conclude that the expression of Syt7 does not promote AR at the CF→PC synapse during and following stimulus trains.

Syt7 and initial P_R at CF→PC synapses

Syt7 can also increase initial P_R, as at the *Drosophila* developing neuromuscular junction (Guan et al., 2020). This has been shown convincingly using an optical approach that allows the determination of P_R for individual release sites. At mammalian synapses, no effect of Syt7 on P_R has been reported, but many of the approaches that have been used are less sensitive than that employed at the *Drosophila* NMJ. Most typically, the EPSC size is quantified, and if the EPSC size is unchanged in Syt7 KO animals, it is inferred that Syt7 does not alter the initial P_R (Bacaj et al., 2013; Turecek et al., 2016). At hippocampal CA3 to CA1 synapses, the use-dependent block of NMDA receptors (NMDARs) was unchanged for single stimuli but significantly faster for multiple stimuli, indicating that Syt7 did not increase initial P_R but increased P_R for subsequent facilitated stimuli (Jackman et al., 2016). In addition, Syt7 did not alter the Ca_e dependence of EPSC amplitude at this synapse, further supporting the lack of effect of Syt7 on initial P_R (Jackman et al., 2016). This suggests that Syt7 influences synaptic transmission by very different mechanisms at most mammalian synapses than is the case at the *Drosophila* NMJ. Here, we find, however, that Syt7 expression also decreases EPSC size at CF→PC synapses, suggesting that high levels of Syt7 can also influence initial P_R at mammalian synapses.

Syt7 increases facilitation at CF→PC synapses

Previous studies of the CF→PC synapse provide insight into the extent to which Syt7 influences short-term plasticity by decreasing P_R to indirectly increase facilitation or by directly promoting facilitation. The key to this issue is the relationship between initial P_R and PPR, which has been determined at the CF→PC synapse by varying Ca_e (Dittman and Regehr, 1998; Foster et al., 2002). The Ca_e dependence of initial EPSC amplitude is well approximated by a power law relationship for $Ca_e < 0.75$ mM but begins to flatten out and eventually plateaus at higher values of Ca_e, in part as a consequence of postsynaptic receptor saturation. Short-term plasticity is also Ca_e dependent. For $Ca_e \leq 0.5$ mM, paired-pulse facilitation is observed, and as Ca_e is elevated, there is a transition to paired-pulse depression for $Ca_e > 0.75$ mM. Further increasing Ca_e leads to more pronounced depression.

In low Ca_e, we find that the Syt7 expression decreases the EPSC amplitude by ~40% and increases facilitation from ~ 58% in control to ~143% (Table S1). We have previously shown that lowering Ca_e to decrease synaptic strength by 50% increased facilitation by less than 20% (Foster et al., 2002). This suggests that changes in P_R are unlikely to account for most of the increase in facilitation produced by Syt7 expression.

For high Ca_e, we find that Syt7 expression produces a dramatic decrease in the extent of depression, such that, for an ISI of 10 ms, PPR is 0.66 when Syt7 is expressed, compared to 0.16 for control experiments (Figure 4A). The initial EPSC amplitude was not significantly different, but there the average EPSC was reduced by ~22% (Table S1). In contrast, lowering Ca_e from 4 mM to 1 mM also changed PPR to ~0.7, but it also decreased EPSC amplitudes by ~50% (Foster et al., 2002). Moreover, lowering Ca_e from 4 mM to 1 mM leads to paired pulse depression for all ISIs (Dittman and Regehr, 1998), whereas we observed paired-pulse facilitation for ISIs of 100 ms to 4 s when we expressed Syt7. These findings suggest that changes in P_R cannot account for the Syt7-dependent changes in PPR in high Ca_e. In addition, the responses evoked by stimulus trains in high Ca_e are not explained by a change in P_R. Reducing P_R by decreasing Ca_e to 1 mM alters responses during trains, but the most obvious effect is that the steady-state responses are depressed to a lesser extent rather than being virtually eliminated (Dittman and Regehr, 1998), as observed for both control and Syt7-expressing synapses in 4 mM Ca_e.

Summary

Thus, we conclude that the primary consequence of introducing Syt7 to CFs, which do not normally express Syt7, is to produce robust facilitation of the CF→PC synapse.

STAR★METHODS

RESOURCE AVAILABILITY

Lead contact—Further information and requests for resources and reagents should be directed to and will be fulfilled by the Lead Contact, Wade Regehr (Wade_Regehr@hms.harvard.edu).

Materials availability—The study did not generate new unique reagents.

Data and code availability

- All data reported in this paper will be shared by the lead contact upon request.
- This paper does not report original code.
- Any additional information required to reanalyze the data reported in this paper is available from the lead contact upon request.

EXPERIMENTAL MODEL AND SUBJECT DETAILS

Mice—Animal procedures were carried out in accordance with NIH guidelines. Protocols were approved by the Harvard Medical Area Standing Committee on Animals. Global Synaptotagmin 7 knockout (Syt7 KO) mice and C57/BL6 mice (Charles River) of either

sex were used for experiments. Syt7KO mice were originally obtained from Jackson Laboratories and maintained with heterozygous breeding pairs. *In situ* hybridization and immunohistochemistry studies were performed using P26-P41 mice. Injections of the inferior olive were performed on P6–9 C57/BL6 mice. Electrophysiological studies were performed using P22–29 mice.

METHOD DETAILS

***In Situ* Hybridization and Immunohistochemistry—**In total, 5 different animals were used for *in situ* hybridization (Figure 2A) and immunohistochemistry (Figures 2B and 2F). For *in situ* hybridization (Figure 2A), one P41 WT animal (Syt7 KO littermate) was anesthetized via isoflurane. The brain was removed and rapidly frozen on dry ice before being embedded in optimal cutting temperature (OCT) compound (Tissue-Tek) and stored at −80°C. 20 μm slices were cut parasagitally on a cryostat (Microm HM500-CM) and mounted with ProLong Gold Antifade (cat# P36934) on Super-frost Plus glass slides. RNAscope® (ACD-Bio) was performed similar to Rudolph et al. (2020) by Mahmoud El-Rifai (Neurobiology Imaging Facility at Harvard Medical School). The image of Figure 2A was obtained with a whole slide scanning microscope (Olympus VS120, 20X air objective). Images were processed and prepared using ImageJ/Fiji and plugins (see Key resources table).

Immunohistochemistry was performed with tissue from ~P40 WT or Syt7 KO mice (Figure 2B), or from P25 ChR2 or ChR2+Syt7 injected C57Bl6 mice (Figure 2F). Mice were anesthetized with ketamine/xylazine and transcardially perfused with phosphate-buffered saline (PBS), followed by 4% paraformaldehyde in phosphate buffered saline (PFA). After brain removal, the tissue was post-fixed in PFA overnight at 4°C. For Figure 2F brains were embedded in low-melting point agarose before cutting. Parasagittal sections of 50 μm were made using a Leica VT1000S vibratome.

For immunostaining, free-floating sections were typically treated with 0.1% Triton X-100 for 10 or 30 minutes, washed in PBS, then followed by 0.1% Triton and 4% normal goat serum for 1 hour at room temperature (NGS, Abcam). After washing in PBS, slices were treated overnight at 4°C with a subset of the following primary antibodies: anti-Syt7 polyclonal rabbit antibody antibody (Synaptic Systems, 105 173; used for WT versus Syt7 KO), diluted 1:200; anti-Syt7 monoclonal mouse antibody (Sigma, MABN665l used for ChR2 versus ChR2+Syt7), diluted 1:200; anti-vesicular glutamate transporter 2 (VGLUT2, Synaptic Systems, 135 404) diluted 1:500. Dilutions were typically made from stock concentrations supplied by vendors. Slices were typically washed three times for 10 minutes at room temperature in 0.1% TritonX and 4% NGS, followed by application of secondary antibodies as listed in the Key resources table for 1 or 2 hours at room temperature. Secondaries were typically diluted 1:500 from stock concentrations supplied by vendors. Slices were then washed with PBS and mounted with ProLong Diamond Antifade (Thermo Fisher Scientific) on glass slides. Images were acquired on an Olympus FluoView1200 confocal microscope using a 60× 1.4 NA oil immersion objective at the Neurobiology Imaging Facility at Harvard Medical School. Images were processed and prepared using Fiji (ImageJ, NIH).

Viruses and stereotaxic injections—AAV9-hSyn-hChR2(H134R)-EYFP was obtained from the University of Pennsylvania Vector Core, or Addgene. AAV9-hSyn-hChR2(H134R)-P2A-Syt7WT were generated previously (Jackman et al., 2016) or by the Boston Children's Vector Core.

Injections of the inferior olive were performed on P6–9 C57/BL6 mice of both sexes. Animals were anesthetized with isoflurane (1%–4%). Viruses were injected using fine capillary glass needles using a Nanoject II or III (Drummond) mounted on a stereotax. Most injections were performed by accessing the inferior olive via the dorsal brainstem (Miyazaki and Watanabe, 2011). For optimal pup survival and injection results, the following steps emerged most useful: achieving head stability using non-rupture ear bars (Kopf), or open-ended cut pipette tips attached to regular ear bars. Keeping dorsal neck skin unshaven and incision size minimal, preferably only cutting one side of neck muscles. The head was aimed kept level while briefly removing support of the body, causing the animal to hang freely from ear bars. Good results were achieved when a capillary glass needle was inserted at ~46° to the perpendicular line with one or more injection sites near (above, at, below) the upper third area of the occipital bone-C1 midline, 0.06–0.1 mm laterally or bilaterally to the midline and ~2mm deep (measured from dura mater). In order to limit virus leakage, we recommend minimizing the size of the dura mater incision and preferably only use a sharp injection needle to break through. Ideally, the injection needle tip should be kept as small as possible. During insertion of the needle, a pocket should be generated by advancing the pipette 0.1 mm further than the target distance to provide a reservoir for virus (advancing needle to 2.1 mm depth and retracting to 2 mm). Ideally, the needle should be paused in place before injection to allow for tissue equilibration. The majority of injections used 300–350 nL of virus suspension per injection site. Ideally, the needle was kept in place for several minutes after injection. Absorbable sutures (e.g., Ethicon Vicryl (Polyglactin 910) Sutures) were used on skin only and applied in both continuous as well as interrupted techniques.

In a subset of experiments, the inferior olive was injected ventrally via the neck. A small incision was made on the ventral neck and the underlying muscle and trachea were gently pushed aside. Bilateral injections of 200–300 nL were made into the ventral brainstem between the occipital bone and C1 vertebrae, 0.05–0.1 mm lateral and 0.2 mm deep. The injection needle was held in place only briefly following injection and then retracted. Following injections pups were thoroughly cleaned and allowed to recover for up to several hours on a heating pad before being returned to their mother or a foster mother.

To increase post-surgical survival CD-1 IGS foster mothers can be very useful. Additional steps to improve survival included familiarizing mothers beforehand with uninjected foster pups, surgery-related smells, rubbing pups in litter, and returning injected pups together with uninjected animals. Best survival results were achieved when returning a litter one-by-one outside of the nest, allowing the mother one-by-one to carry them into the nest.

Slice preparation—Injected animals or WT and Syt7 KOs (P22–29 mice of either sex) were anesthetized using isoflurane and decapitated. The cerebellum was dissected in ice-cold solution consisting of (in mM): 110 Choline-Cl, 7 $MgSO_4$ or $MgCl_2$, 2.5 KCl, 1.2 NaH_2PO_4, 0.5 $CaCl_2$, 25 glucose, 11.6 Na-Ascorbate, 2.4 Na-Pyruvate and 25 $NaHCO_3$,

oxygenated with 95% O2, 5% CO2. Parasagittal slices of cerebellum were made using a Leica VT1200S vibratome. Slices were then transferred to the holding chamber with ACSF containing (in mM): 125 NaCl, 26 $NaHCO_3$, 1.25 NaH_2PO_4, 2.5 KCl, 25 glucose, 1.5 $CaCl_2$ and 1.5 $MgCl_2$, oxygenated with 95% O2, 5% CO2. Slices were maintained at 32–34°C for around 15–30 minutes before being allowed to incubate at room temperature. For experiments, slices were transferred to the recording chamber. In experiments comparing WT and Syt7 KO mice in high Ca_e (Figure 1C), P12–14 mice were prepared as described above, but with transcardial perfusion and solution containing (in mM): 250 sucrose, 2.5 KCl, 1.25 NaH2PO4, 25 NaHCO3, 10 Glucose, 7 MgCl2, 0.5 CaCl2, oxygenated with 95% O2, 5% CO2.

Electrophysiology—Brain slices were transferred from the holding chamber and mounted onto poly-L-lysine coated coverslips with holding chamber ACSF. They were submerged in the recording chamber by oxygenated recirculating (e.g., 100 ml) recording ACSF consisting of (in mM): 125 NaCl, 26 $NaHCO_3$, 1.25 NaH_2PO_4, 2.5 KCl, 25 glucose, oxygenated with 95% O2, 5% CO2, with divalent concentrations adjusted for each experiment. For low external calcium experiments, recording ACSF consisted of ~0.3 mM Ca and 2.7 mM MgCl2. For high external calcium experiments, recording ACSF was made to consist of ~4 mM Ca and 0 mM MgCl2, with the exception of Figure 1C, for which recording ACSF consisted of 4 mM Ca and 1 mM MgCl2. Experiments were conducted in the presence of picrotoxin (100 μM) or bicuculine (20 μM). For experiments in high Ca_e, 300 nM NBQX was added to minimize unclamped EPSCs. Recordings were made with borosilicate thick-walled glass electrodes filled with (in mM): 100 CsCl, 35 CsF, 10 EGTA, 10 HEPES, 5 QX-314 (Weyrer et al., 2019). Recordings were collected at 10–20 kHz filtered at 10kHz using a Multiclamp 700B (Molecular Devices) and digitized with an ITC-18 using mafPC (courtesy of Matthew A. Xu-Friedman) and custom procedures (courtesy of Skyler L. Jackman) in IgorPro (Wavemetrics). Cells were held at −40 mV. Series resistance was typically compensated up to 80%. Climbing fibers were electrically stimulated using a theta-glass or fine-tipped monopolar glass electrode (only for Figure 1C) placed in the granule cell layer near the PC soma and were distinguished from parallel fibers by their all-or-none nature.

Experiments in Figures 1 and S1, were performed with Syt7 KO animals and WT controls. Recordings in Figures 1A, 1B, and S1 were performed blind to genotype. Viral expression experiments were performed in wild-type animals and a subset of recordings were performed blind to phenotype.

Optogenetics—Climbing fibers expressing ChR2-YFP were optically stimulated with 470 nm light from an LED (Thorlabs, Cat# M470L3; 650 mW). An advantage of the CF to PC synapse is that there is generally a single CF synapse onto a PC for our recording age range. This input can be stimulated in an all-or-none manner, and the approach does not require viral expression in the same number of fibers to compare CF synapses expressing ChR2 alone with those expressing ChR2 + Syt7. We included cells in which the CF input could be activated in an all-or-none manner both electrically and optically, and for which there was good agreement between the amplitudes and time courses of optical and electrical EPSCs,

and the ability to adequately follow optical stimulation. Optical stimulation intensity was >80 mW/mm^2 with a duration of 0.1–1ms. Figure 2E shows low Ca_{ext} responses with an applied optical pulse width of 1ms. We interpreted optical activation to indicate sufficient ChR2-YFP expression and therefore Syt7 expression. Light intensity was determined with a VEGA Ophir power-meter.

Analysis—Data were analyzed using custom scripts written in MATLAB (Mathworks; by Tomas Osorno Ferro and C.W.), IgorPro (mainly courtesy of Skyler L. Jackman) and Microsoft Excel, available upon request. For presented data (except Figure 2E), stimulus artifacts were blanked for clarity.

EPSC amplitudes were measured as the peak current following stimulation, with the baseline measured just prior to the stimulus onset. During high frequency stimulation or when ISIs were small, EPSCs did not fully decay between stimuli. For PPR, for short ISIs the amplitude of EPSC2 was determined by subtracting EPSC1 collected for longer ISI trials. For trains (after EPSC1) the baseline was measured by extrapolating a single (low Ca_e) or double (high Ca_e) exponential fit to the previous EPSC. For EPSC11 in Figures 4F and 4G, the baseline was collected just prior to the stimulus onset. For 50 Hz trains in high Ca_e (Figures 4B, 4E–4G, S5E, and S5F) later EPSCs often became asynchronous. As a result, if fits seemed too unrealistic, very few individual EPSC measurements were excluded. In addition, the time to look for peak EPSC after stimulus 10 for the high Ca_e 50 Hz experiments was limited to the ISI of 20 ms. For some experiments, intervals were 0.05 ms off (e.g., 100 ms ISI was actually a 99.95 ms ISI). Those cells/trials were pooled (if needed) with the rest of the experiments.

We defined half decay time of a measured EPSC as the time needed to reach half of the amplitude between the baseline (measured before stimulus onset of EPSC1) and the peak EPSC (EPSC1, EPSC2 (of a 20 ms ISI stimulation) or EPSC10). EPSCs were fit with a double exponential and the half decay time of the double exponential fit was collected as the time needed until the double exponential fit reached half of the peak-baseline (before EPSC1) amplitude.

Normalization was performed to illustrate potential differences in EPSC decay. For PPR For PPR experiments, we normalized to the peak of EPSC1 or the peak of EPSC2 (of a 20 ms ISI stimulation). For high frequency trains we usually normalized to the peak of EPSC10. For correct comparisons, the peaks of two final normalized control and Syt7 averages were aligned if needed (e.g., small differences in latency). 50 Hz trains in high calcium often showed asynchronous release especially in the later EPSCs. To minimize EPSC10 decay misalignment, minimal negative EPSC value was detected only within a 8 ms time window (40% of ISI).

QUANTIFICATION AND STATISTICAL ANALYSIS

Statistics were performed using Graphpad Prism and statistical tests are indicated in Table S1. Usually statistics were performed using unpaired two-tailed Student’s t test (see Table S1) with a significance level of $p < 0.05$ (*). Same standard deviation was assumed for both tested populations. Figures typically show a scatterplot with mean ± SEM Table

S1 shows all presented experiments as number of cells (n) and number of animals (N). Measurements are typically presented as mean ± SEM. For figures, PPR and train data was further visualized by applying various fits (via IGOR Pro) to the data points (see Table S2). For Figure 4, double exponential (Control in Figures 4A–4D and in Figure 4F (stimuli 1–10)), lognormal peak shape (Syt7 in Figures 4A and 4D), sigmoid function (Syt7 in Figure 4B and in Figure 4F) and Hill's equation (Syt7 in Figure 4C). For the 11th and 12th EPSC in Figure 4F Control and Syt7 we fitted lines.

Supplementary Material

Refer to Web version on PubMed Central for supplementary material.

ACKNOWLEDGMENTS

This work was supported by a NIH grant R35NS097284 to W.G.R., a Boehringer Ingelheim Fonds PhD Fellowship, the B&C Privatstiftung, and Alice and Joseph Brooks Postdoctoral Fellowship to C.W. We thank the Regehr lab, especially T. Osorno, S. Rudolph, S. Jackman, and K. McDaniels, for helping with experiments and analysis. Imaging was performed in the Vision Core and NINDS P30 Core Center (NS072030 to the Neurobiology Imaging Center at Harvard Medical School) with the help of M. El-Rifai (performed RNA scope) and M. Ocana.

REFERENCES

Atluri PP, and Regehr WG (1998). Delayed release of neurotransmitter from cerebellar granule cells. J. Neurosci 18, 8214–8227. [PubMed: 9763467]

Bacaj T, Wu D, Yang X, Morishita W, Zhou P, Xu W, Malenka RC, and Südhof TC (2013). Synaptotagmin-1 and synaptotagmin-7 trigger synchronous and asynchronous phases of neurotransmitter release. Neuron 80, 947–959. [PubMed: 24267651]

Best AR, and Regehr WG (2009). Inhibitory regulation of electrically coupled neurons in the inferior olive is mediated by asynchronous release of GABA. Neuron 62, 555–565. [PubMed: 19477156]

Chen C, Satterfield R, Young SM Jr., and Jonas P (2017). Triple function of synaptotagmin 7 ensures efficiency of high-frequency transmission at central GABAergic synapses. Cell Rep. 21, 2082–2089. [PubMed: 29166601]

DiAntonio A, and Schwarz TL (1994). The effect on synaptic physiology of synaptotagmin mutations in Drosophila. Neuron 12, 909–920. [PubMed: 7909234]

Dittman JS, and Regehr WG (1998). Calcium dependence and recovery kinetics of presynaptic depression at the climbing fiber to Purkinje cell synapse. J. Neurosci 18, 6147–6162. [PubMed: 9698309]

Fernández-Chacón R, Königstorfer A, Gerber SH, García J, Matos MF, Stevens CF, Brose N, Rizo J, Rosenmund C, and Südhof TC (2001). Synaptotagmin I functions as a calcium regulator of release probability. Nature 410, 41–49. [PubMed: 11242035]

Foster KA, Kreitzer AC, and Regehr WG (2002). Interaction of postsynaptic receptor saturation with presynaptic mechanisms produces a reliable synapse. Neuron 36, 1115–1126. [PubMed: 12495626]

Geppert M, Goda Y, Hammer RE, Li C, Rosahl TW, Stevens CF, and Südhof TC (1994). Synaptotagmin I: a major Ca2+ sensor for transmitter release at a central synapse. Cell 79, 717–727. [PubMed: 7954835]

Guan Z, Quiñones-Frías MC, Akbergenova Y, and Littleton JT (2020). *Drosophila* Synaptotagmin 7 negatively regulates synaptic vesicle release and replenishment in a dosage-dependent manner. eLife 9, e55443. [PubMed: 32343229]

Hull C (2020). Prediction signals in the cerebellum: beyond supervised motor learning. eLife 9, e54073. [PubMed: 32223891]

Huson V, and Regehr WG (2020). Diverse roles of Synaptotagmin-7 in regulating vesicle fusion. Curr. Opin. Neurobiol 63, 42–52. [PubMed: 32278209]

Jackman SL, and Regehr WG (2017). The mechanisms and functions of synaptic facilitation. Neuron 94, 447–464. [PubMed: 28472650]

Jackman SL, Turecek J, Belinsky JE, and Regehr WG (2016). The calcium sensor synaptotagmin 7 is required for synaptic facilitation. Nature 529, 88–91. [PubMed: 26738595]

Kochubey O, and Schneggenburger R (2011). Synaptotagmin increases the dynamic range of synapses by driving Ca^2+-evoked release and by clamping a near-linear remaining Ca^2+ sensor. Neuron 69, 736–748. [PubMed: 21338883]

Littleton JT, Stern M, Schulze K, Perin M, and Bellen HJ (1993). Mutational analysis of Drosophila synaptotagmin demonstrates its essential role in Ca(2+)-activated neurotransmitter release. Cell 74, 1125–1134. [PubMed: 8104705]

Liu H, Bai H, Hui E, Yang L, Evans CS, Wang Z, Kwon SE, and Chapman ER (2014). Synaptotagmin 7 functions as a Ca2+-sensor for synaptic vesicle replenishment. eLife 3, e01524. [PubMed: 24569478]

Luo F, and Südhof TC (2017). Synaptotagmin-7-mediated asynchronous release boosts high-fidelity synchronous transmission at a central synapse. Neuron 94, 826–839.e3. [PubMed: 28521135]

MacDougall DD, Lin Z, Chon NL, Jackman SL, Lin H, Knight JD, and Anantharam A (2018). The high-affinity calcium sensor synaptotagmin-7 serves multiple roles in regulated exocytosis. J. Gen. Physiol 150, 783–807. [PubMed: 29794152]

Miyazaki T, and Watanabe M (2011). Development of an anatomical technique for visualizing the mode of climbing fiber innervation in Purkinje cells and its application to mutant mice lacking GluRδ2 and Ca(v)2.1. Anat. Sci. Int 86, 10–18. [PubMed: 21153457]

Neher E (2015). Merits and limitations of vesicle pool models in view of heterogeneous populations of synaptic vesicles. Neuron 87, 1131–1142. [PubMed: 26402599]

Rudolph S, Guo C, Pashkovski SL, Osorno T, Gillis WF, Krauss JM, Nyitrai H, Flaquer I, El-Rifai M, Datta SR, and Regehr WG (2020). Cerebellum-specific deletion of the $GABA_A$ receptor δ subunit leads to sex-specific disruption of behavior. Cell Rep. 33, 108338. [PubMed: 33147470]

Sakaba T, and Neher E (2001). Calmodulin mediates rapid recruitment of fast-releasing synaptic vesicles at a calyx-type synapse. Neuron 32, 1119–1131. [PubMed: 11754842]

Stevens CF, and Wesseling JF (1998). Activity-dependent modulation of the rate at which synaptic vesicles become available to undergo exocytosis. Neuron 21, 415–424. [PubMed: 9728922]

Sun J, Pang ZP, Qin D, Fahim AT, Adachi R, and Südhof TC (2007). A dual-Ca2+-sensor model for neurotransmitter release in a central synapse. Nature 450, 676–682. [PubMed: 18046404]

Thanawala MS, and Regehr WG (2016). Determining synaptic parameters using high-frequency activation. J. Neurosci. Methods 264, 136–152. [PubMed: 26972952]

Turecek J, and Regehr WG (2019). Neuronal regulation of fast synaptotagmin isoforms controls the relative contributions of synchronous and asynchronous release. Neuron 101, 938–949.e4. [PubMed: 30733150]

Turecek J, Jackman SL, and Regehr WG (2016). Synaptic specializations support frequency-independent Purkinje cell output from the cerebellar cortex. Cell Rep. 17, 3256–3268. [PubMed: 28009294]

Turecek J, Jackman SL, and Regehr WG (2017). Synaptotagmin 7 confers frequency invariance onto specialized depressing synapses. Nature 551, 503–506. [PubMed: 29088700]

Wadiche JI, and Jahr CE (2001). Multivesicular release at climbing fiber-Purkinje cell synapses. Neuron 32, 301–313. [PubMed: 11683999]

Wang LY, and Kaczmarek LK (1998). High-frequency firing helps replenish the readily releasable pool of synaptic vesicles. Nature 394, 384–388. [PubMed: 9690475]

Wen H, Linhoff MW, McGinley MJ, Li GL, Corson GM, Mandel G, and Brehm P (2010). Distinct roles for two synaptotagmin isoforms in synchronous and asynchronous transmitter release at zebrafish neuromuscular junction. Proc. Natl. Acad. Sci. USA 107, 13906–13911. [PubMed: 20643933]

Weyrer C, Turecek J, Niday Z, Liu PW, Nanou E, Catterall WA, Bean BP, and Regehr WG (2019). The Role of Ca_V2.1 Channel Facilitation in Synaptic Facilitation. Cell Rep. 26 (9), 2289–2297. [PubMed: 30811980]

Xu-Friedman MA, Harris KM, and Regehr WG (2001). Three-dimensional comparison of ultrastructural characteristics at depressing and facilitating synapses onto cerebellar Purkinje cells. J. Neurosci 21, 6666–6672. [PubMed: 11517256]

Highlights

- The climbing fiber (CF) to PC synapse is unaltered in synaptotagmin 7 (Syt7) KO mice
- CFs lack Syt7 in wild-type animals
- Expressing Syt7 in CFs strongly increases facilitation at CF to PC synapses
- Expressing Syt7 does not affect recovery from depression or asynchronous release

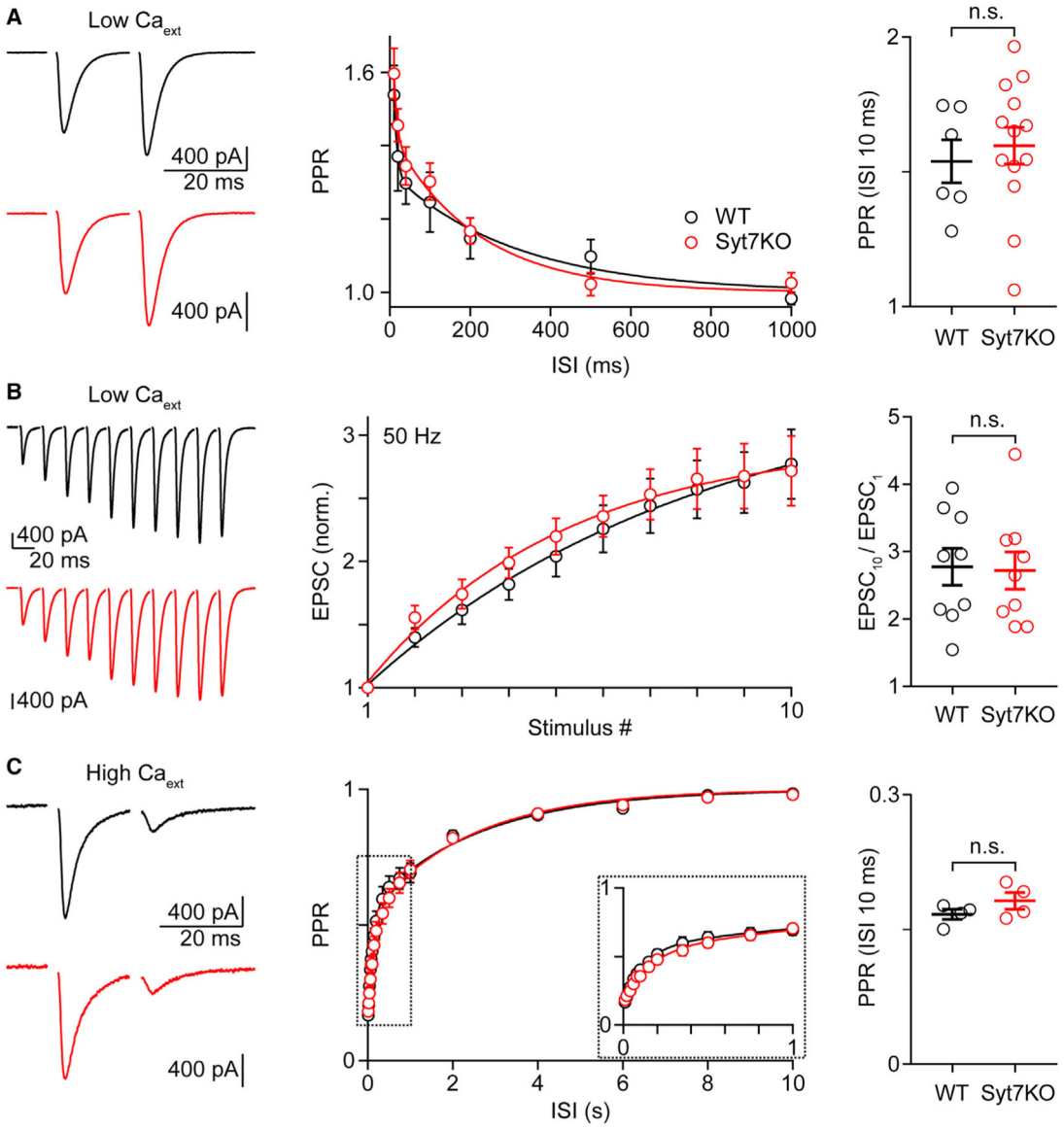

Figure 1. Properties of the CF→PC synapse do not depend on synaptotagmin 7 in wild-type animals

(A–C) Experiments were performed in wild-type (WT) (black) and synaptotagmin 7 knockout (Syt7 KO) animals at the CF-PC synapse under conditions of low (A and B; ~0.3 mM) or high (C; ~4 mM) external calcium (Ca_e). (Left) Representative EPSCs with an inter-stimulus interval (ISI) of 20 ms (A and C) or evoked by a 50-Hz train (B) are shown. (Middle) The average paired-pulse ratio (PPR) is plotted as function of the ISI (A and C). The zoomed-in inset is indicated by dashed rectangles (C). The summary for the normalized average EPSC amplitudes is shown for the 50-Hz train (B). (Right) Plots with indicated mean ± SEM for the PPR at 10 ms (A and C) and the ratio $EPSC_{10}/EPSC_1$ (B) are shown. Statistical significance (unpaired t test; see Tables S1): not significant (n.s.). Data are shown as mean ± SEM. See also Tables S1 and S2 and Figure S1.

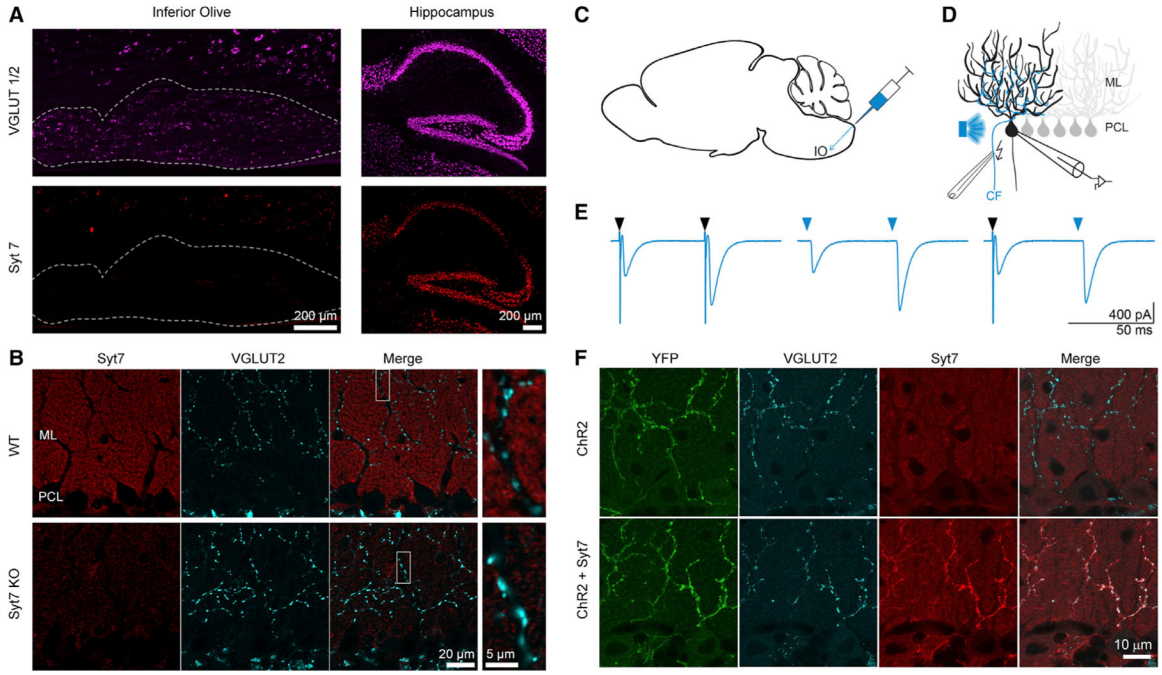

Figure 2. Syt7 expression in climbing fibers (CFs) with adeno-associated virus (AAV) infection of the inferior olive used to express Syt7 in CFs

(A) Fluorescent *in situ* hybridization of WT mouse: labeling of vesicular glutamate transporter 1 and 2 (VGLUT1/2; magenta) and Syt7 (red) is shown in parasagittal slices for the inferior olive (IO) (left; dashed outline) and the hippocampus (right). ML, molecular layer; PCL, Purkinje cell layer. Both scale bars are 200 µm.

(B) Immunohistochemistry of WT (top) and Syt7 KO (bottom) parasagittal cerebellar slices. Syt7 (red), VGLUT2 (cyan), and the merge of the 2 channels are shown. The scale bar on the left is 20 µm, and the right scale bar is 5 µm.

(C) Schematic of intracranial brain injections of AAV9-ChR2 or AAV9-ChR2-Syt7 via the back approach targeting the IO (see STAR Methods).

(D) Schematic of the experimental electrophysiological recording setup in which AAV-infected CFs were identified by optical stimulation and experimentally tested by electric stimulation.

(E) Responses are shown for an AAV9-ChR2-Syt7-infected CF-PC synapse, following optical (light blue arrow) or electrical (black arrow) stimulation.

(F) Immunohistochemistry shows CF infection with AAV9-ChR2 (upper) and AAV9-ChR2-Syt7 (lower). The scale bar is 10 µm.

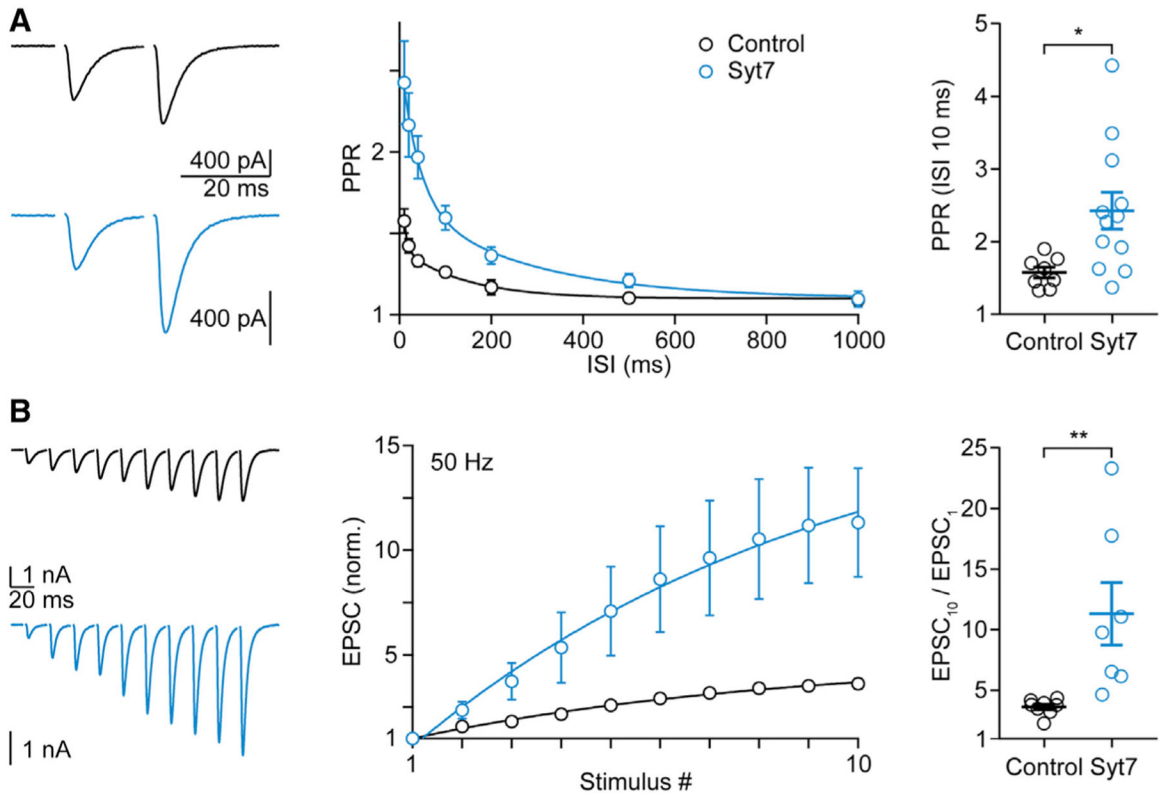

Figure 3. Viral expression of Syt7 in CFs increases paired-pulse and train facilitation at CF to PC synapses in low Ca_e

(A and B) Paired-pulse (A) and train (B) facilitation experiments were performed in ChR2- (black) and Syt7-ChR2 (light blue)-injected animals at the CF-PC synapse under conditions of low (~0.3 mM) external calcium. (Left) Representative EPSCs with an ISI of 20 ms (A) or evoked by a 50-Hz train (B) are shown. (Middle) The average PPR is plotted as function of the ISI (A), and the summary for the normalized average EPSC amplitudes is shown for the 50-Hz (B) train. (Right) Mean ± SEM for the PPR at 10 ms (A) and the ratio $EPSC_{10}/EPSC_1$ (B) are shown. Statistical significance (unpaired t test; see Table S1): *p < 0.05; **p < 0.01. Data are shown as mean ± SEM. See also Table S1 and Figures S2–S4.

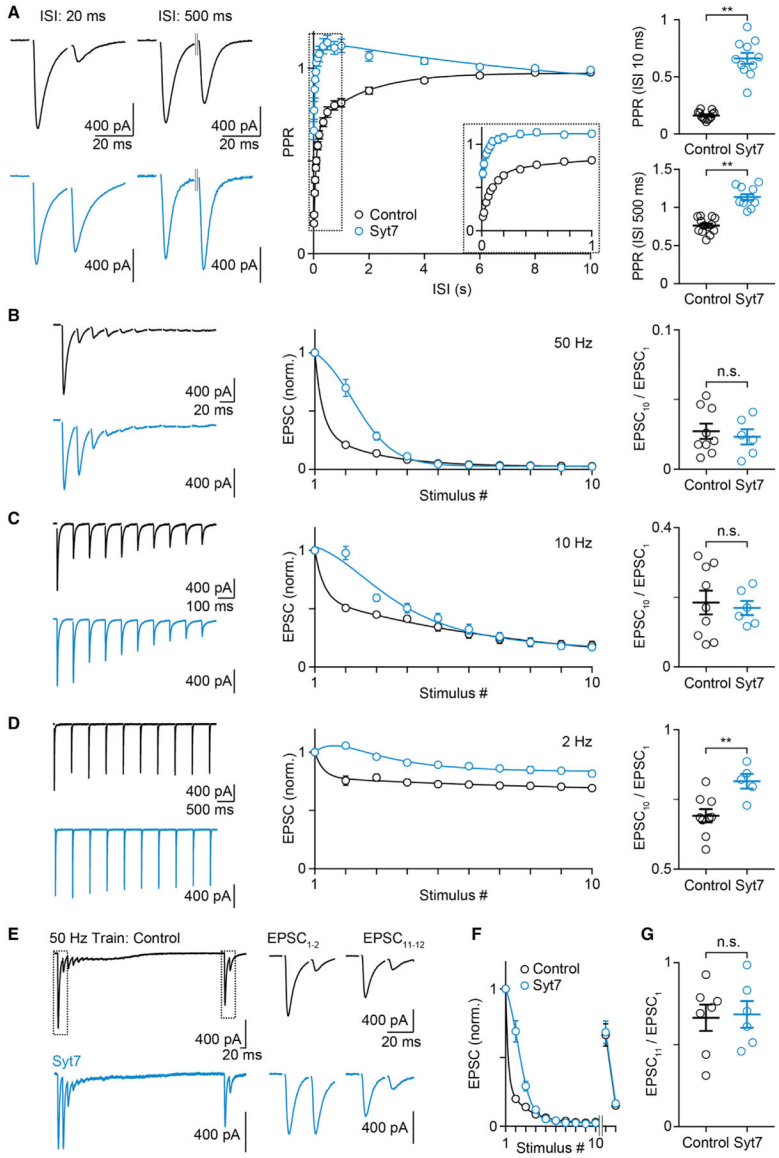

Figure 4. In high external calcium, Syt7 expression in CFs leads to changes in PPR and high-frequency trains without altering recovery after depletion

Experiments were performed in ChR2- (black) and Syt7-ChR2 (light blue)-injected animals at the CF-PC synapse in 4 mM Ca_e.

(A–D) (Left) Representative EPSCs with an ISI of 20 ms (A, left), 500 ms (A, middle left), or EPSCs evoked by a 50-Hz (B), 10-Hz (C), or 2-Hz (D) train are shown. (Middle) The average PPR is plotted as function of the ISI (A), and summaries for the normalized average EPSC amplitudes are shown for 50 Hz (B), 10 Hz (C), and 2 Hz (D) trains. (Right) Mean ± SEM for the PPR at 10 and 500 ms (A) and the $EPSC_{10}/EPSC_1$ ratio (B–D) are shown.

(E) Responses evoked by a 50-Hz train (EPSCs 1–10) followed by a 500-ms pause and then with a pair of pulses with a 20-ms ISI (EPSCs 11 and 12).

(F) Summary for experiments as in (E).

(G) Summary of mean ± SEM for $EPSC_{11}$ / $EPSC_1$.

Statistical significance (unpaired t test; see Table S1): n.s.; **$p < 0.01$. Data are shown as mean ± SEM. Fits are as mean ± SD. See also Figure S5 and Table S1.

KEY RESOURCES TABLE

REAGENT or RESOURCE	SOURCE	IDENTIFIER
Antibodies		
Rabbit Anti-Syt7	Synaptic Systems	Synaptic Systems Cat# 105 173; RRID:AB_887838
Mouse Anti-Syt7 N275-14	Neuromab/Sigma	Millipore Cat# MABN665; RRID:AB_2888943
Guinea Pig Anti-vesicular glutamate transporter 2 (VGLUT2)	Synaptic Systems	Synaptic Systems Cat# 135 404; RRID:AB_887884
Anti-rabbit Alexa Fluor 647	Abcam	Abcam Cat# ab150083; RRID:AB_2714032
Anti-guinea-pig Alexa Fluor 488	Abcam	Abcam Cat#ab150185; RRID:AB_2736871
Anti-mouse Alexa Fluor 647	Abcam	Abcam Cat#ab150115; RRID:AB_2687948
Anti-Guinea-pig Alexa Fluor 555	Abcam	Abcam Cat#ab150186
Goat-anti-GFP FITC	Abcam	Abcam Cat# ab6662; RRID:AB_305635
Chemicals, peptides, and recombinant proteins		
NBQX disodium salt	Abcam	ab120046
Picrotoxin	Abcam	ab120315
(+)-Bicuculline	Sigma	14340
QX-314 Cl	Abcam	ab120118
Experimental models: organisms/strains		
C57BL/6, *Mus musculus*	Charles River	N/A
CD-1 IGS, *Mus musculus*	Charles River	N/A
Syt7 Global Knockout B6.129S1-*Syt7*$^{tm\ 1Nan}$/J	Jackson Labs	IMSR Cat# JAX:004950; RRID:IMSR_JAX:004950
Oligonucleotides		
RNAscope® Probe - Mm-Syt7-C2	ACD-Bio	546201-C2
RNAscope® Probe - Mm-Slc17a7-C3	ACD-Bio	416631-C3
RNAscope® Probe - Mm-Slc17a6-C3	ACD-Bio	319171-C3
Recombinant DNA		
AAV9-hSyn-hChR2(H134R)-EYFP	University of Pennsylvania Vector Core /Addgene	26973-AAV9
AAV9-hSyn-hChR2(H134R)-EYFP-P2A-Syt7WT	Boston Children's Vector Core	N/A
Software and algorithms		
MATLAB	Mathworks	RRID:SCR_001622
IgorPro	Wavemetrics	RRID:SCR_000325
ImageJ/Fiji software	NIH/Fiji	RRID: SCR_002285
GraphPad Prism 7	GraphPad	RRID: SCR 002798
FluoView software	Olympus	RRID:SCR_014215
OlyVIA	Olympus	RRID:SCR_016167
Microsoft Excel	Microsoft	RRID:SCR_016137
MultiClamp 700B Commander	Molecular Devices / Axon Instruments	RRID:SCR_018455
Adobe Illustrator	Adobe	RRID:SCR_010279

REAGENT or RESOURCE	SOURCE	IDENTIFIER
Action bar for ImageJ	By Jérôme Mutterer; "Custom toolbars and mini applications with Action Bar."	https://figshare.com/articles/dataset/Custom_toolbars_and_mini_applications_with_Action_Bar/3397603/3
VSI Reader Actionbar (for ImageJ)	By Olivier Burri, Romain Guiet, Arne Seitz via Biolmaging & Optics Platform (BIOP) of the Ecole polytechnique fédérale de Lausanne (EPFL)	https://www.epfl.ch/research/facilities/ptbiop/